Nanoscale

Scalable Synthesis of Nanoporous Atomically Thin Graphene Membranes for Dialysis and Molecular Separations via Facile Iso-propanol-Assisted Hot Lamination

Journal:	*Nanoscale*
Manuscript ID	NR-COM-10-2020-007384.R1
Article Type:	Communication
Date Submitted by the Author:	14-Dec-2020
Complete List of Authors:	Cheng, Peifu; Vanderbilt University, Moehring, Nicole; Vanderbilt University idrobo, Juan; Oak Ridge National Laboratory, Ivanov, Ilia; Oak Ridge National Laboratory, Center for Nanophase Materials Science Kidambi, Piran Ravichandran; Vanderbilt University, Department of Chemical and Biomolecular Engineering

COMMUNICATION

Scalable Synthesis of Nanoporous Atomically Thin Graphene Membranes for Dialysis and Molecular Separations via Facile Isopropanol-Assisted Hot Lamination

Received 00th January 20xx,
Accepted 00th January 20xx

DOI: 10.1039/x0xx00000x

Peifu Cheng,[a] Nicole K. Moehring,[ab] Juan Carlos Idrobo,[c] Ilia N. Ivanov[c] and Piran R. Kidambi*[abd]

Abstract: Scalable graphene synthesis and facile large-area membrane fabrication are imperative to advance nanoporous atomically thin membranes (NATMs) for molecular separations. Although chemical vapor deposition (CVD) allows for roll-to-roll high-quality monolayer graphene synthesis, facile transfer with atomically clean interfaces to porous supports for large-area NATM fabrication remains extremely challenging. Sacrificial polymer scaffolds commonly used for graphene transfer typically leave polymer residues detrimental to membrane performance and transfers without polymer scaffolds suffer from low yield resulting in high non-selective leakage through NATMs. Here, we systematically study the factors influencing graphene NATM fabrication and report on a novel roll-to-roll manufacturing compatible isopropanol-assisted hot lamination (IHL) process that enables scalable, facile and clean transfer of CVD graphene on to polycarbonate track etched (PCTE) supports with coverage ≥99.2%, while preserving support integrity/porosity. We demonstrate fully functional centimeter-scale graphene NATMs that show record high permeances (~2-3 orders of magnitude higher) and better selectivity than commercially available state-of-the-art polymeric dialysis membranes, specifically in the 0-1000 Da range. Our work highlights a scalable approach to fabricate graphene NATMs for practical applications and is fully compatible with roll-to-roll manufacturing processes.

1 Introduction

Graphene, a single layer of carbon atoms arranged in a hexagonal lattice[1] represents an ideal membrane material,[2,3] with potential for transformative advances in gas separation,[4–7] nanofiltration,[8,9] desalination,[10,11] ionic/molecular separation,[12–20] proton transport,[21,22] DNA translocation,[23,24] dialysis and protein desalting,[3,14] among others. To realize such applications, scalable cost-effective synthesis of high-quality graphene and subsequent membrane fabrication via transfer to an appropriately porous support are imperative. Although roll-to-roll synthesis of high-quality graphene has been demonstrated via CVD on commercially available polycrystalline Cu foils,[25–27] facile transfer of large-area CVD graphene with atomically clean interfaces to appropriately porous supports (without compromising the support integrity/porosity) for NATM fabrication remains non-trivial and extremely challenging.[28]

The electronics community initially leveraged advances in lithography and adapted the use of sacrificial polymer scaffold layers, such as poly(methyl methacrylate) (PMMA),[27] poly(bisphenol A carbonate) (PC),[29] ethylene-vinyl acetate,[30] pentacene,[31] paraffin,[32] parylene[33] among others to transfer CVD graphene onto arbitrary substrates for fabricating devices. Polymer scaffolds allow for large-area crack-free graphene transfer,[25–27] but inevitably leave polymer residues.[34–39] While approaches such as critical point drying[40] and thermal annealing in the presence of H_2 at 200-500 °C allow for the removal of polymer residue to a good extent, complete elimination of polymer residue has proven elusive.[36–39] Further, the combination of high annealing temperatures, presence of H_2 (and/or trace contaminants in H_2) and the surface chemistry of the substrate can lead to un-desired defect formation/modification in the graphene lattice.[35,41–44] The effect of such nanoscale defects and polymer residues is greatly exacerbated for membranes compared with electronic devices,[45] *i.e. i)* a single large nanoscale defect would be relatively un-noticed in most electronic devices but can severely compromise membrane performance via non-selective leakage,[19] and *ii)* polymer residues could also significantly influence transport through NATMs via surface adsorption of species and/or plugging of useful nanopores as well as blocking support pores.[2,3,15,46]

Initial studies on graphene membranes inadvertently utilized polymer-based transfer methods for gas separation,[47,48] desalination,[11] ionic transport,[16,17,49] DNA translocation,[23] and others.[18,50] Indeed, polymer residues and contaminations were found to significantly influence transport through atomically thin

[a] Department of Chemical and Biomolecular Engineering, Vanderbilt University, Nashville, Tennessee 37212, United States. E-mail: piran.kidambi@vanderbilt.edu
[b] Interdisciplinary Materials Science Program, Vanderbilt University, Nashville, Tennessee 37212, United States
[c] Center for Nanophase Materials Sciences, Oak Ridge National Laboratory, Oak Ridge, Tennessee 37831, United States
[d] Department of Mechanical Engineering, Vanderbilt University, Nashville, Tennessee 37212, United States
† Electronic Supplementary Information (ESI) available.

membranes as elegantly highlighted by Rollings et al.[17] by using monolayer graphene transferred onto perforated silicon nitride/Si substrates. Specifically, they reported K^+/Cl^- selectivity > 100 through graphene nanopores as large as 20 nm in diameter under applied potential and attributed it to pH-dependent negative surface charges attached to the hydrocarbon contaminants from the polymer residues.[17] These and other results[20] emphasize the importance of clean graphene transfer with minimal contamination or polymer residue for large-area NATM applications.

Interestingly, Regan et al.[51] showed that evaporation of a drop of isopropanol (IPA) at the interface between CVD graphene and holey carbon coated transmission electron microscopy (TEM) grids allowed for clean transfer of graphene (after acid etch of the Cu foil), albeit some minor cracks in the graphene were observed.[51] O'Hern et al.[12] also showed that a simple manual press of CVD graphene on Cu foils onto PCTE supports at room temperature followed by acid etch of Cu, allowed for graphene transfer with minimal polymer residue and/or contaminants. However, the coverage of graphene obtained was only ~60-80% and necessitated interfacial polymerization (IP) based sealing approaches for NATM fabrication.[12,45] Huang et al.[4] reported on a crack-free transfer of graphene with nanoporous carbon (NPC) films via the pyrolysis of block co-polymers. However, significant post-processing including high temperature pyrolysis (~500 °C) offers limited scalability.[4] Polyether sulfone (PES) casting approaches[15,25,52] were also developed for graphene transfer, but the interconnected pores formed in the PES supports present challenges for IP based sealing of tears in NATMs.[19] Other methods such as using single-walled carbon nanotubes supports and mesoporous silica[8] have also been demonstrated for graphene membranes, but only allow for limited manufacturing scalability. Hence, high-yield transfer of clean large-area graphene onto appropriately porous supports (without compromising support porosity/integrity) using scalable processes for membrane applications remains elusive.

Here, we systematically study the factors influencing scalable roll-to-roll manufacturing compatible fabrication of centimeter-scale NATMs. We evaluate transfer of CVD graphene onto model supports (PCTE supports with ~200 nm pores) using manual compression, mechanical press and scalable lamination. The decoupling of CVD graphene from the Cu foil via water-induced oxidation is found to aid transfer. However, water-induced oxidation significantly damages (~10%) graphene along wrinkles. We demonstrate a novel roll-to-roll manufacturing compatible isopropanol-assisted hot lamination (IHL) process that enables facile, clean and scalable transfer of large-area graphene with coverage ≥ 99.2% without compromising PCTE porosity/integrity and represents the best values reported for centimeter-scale graphene membranes. The < 0.8% leakage is attributed to ≥50 nm defects and/or tears along wrinkles in the CVD graphene. Using facile oxygen plasma etch to form nanopores in the graphene transferred onto PCTE, we demonstrate fully functional NATMs that show ~2-3 orders of magnitude higher permeance and better selectivity than state-of-the-art commercial dialysis membranes (0-1000Da range).

2 Results and discussion

Here, we systematically study the factors influencing fabrication of centimeter-scale NATMs by transferring CVD graphene onto to model PCTE supports (Fig. 1A). We specifically choose PCTE with cylindrical pores ~200 nm diameter as model supports due to *i)* its smooth hydrophobic surface ensuring conformal contact during transfer as well as preventing the wicking in of acid at the graphene/PCTE interface during Cu etch,[12,53] and *ii)* the parallel, well-defined channels in PCTE that effectively prevent cross-talk from overlapping pores and allow for unambiguous interpretation of transport through the synthesized NATMs.[2,3] Scanning electron microscopy (SEM) image of the as-synthesized monolayer graphene on Cu (Fig. 1E) shows graphene wrinkles (~3% of total area, formed due to differences in thermal expansion between graphene and Cu during cooling after CVD) indicating complete film coverage.[45] Raman spectrum I_D/I_G ~ 0.027 (Fig. 1B) and large-area Raman maps (Fig. 1C,D) indicate high-quality monolayer graphene.[54]

For CVD graphene transfer, PCTE is contacted against graphene on Cu foil (G/Cu, with the back-side graphene removed via pre-etch) and sandwiched between two pieces of weighing paper to make a paper/PCTE/G/Cu/paper stack (Fig. 1A). Next, manual compression, cold/hot lamination, and cold/hot press is used to achieve uniform contact between G/Cu and PCTE substrate to promote adhesion and finally the Cu is carefully etched (Fig. 1A,F). The overlapping area of PCTE/G/Cu shows a uniform reddish color (Fig. 1F), indicating macroscopically uniform contact was achieved with the methods described above. Successful fabrication of atomically thin membranes via graphene transfer was achieved (see uniform graphene square attached on PCTE support in Fig. 1F) when the uniform reddish color was maintained during Cu etch, indicating no acid entry at the PCTE and G/Cu interface (see image with a green boundary in Fig. 1F).[12,53] However, incorrect handling (non-conformal contact or submerging the entire stack in the etchant) of the PCTE/G/Cu/paper stack while etching resulted in acid entry at the interface between PCTE and G/Cu, identified by the change in color from reddish to brown and black (see image with a red boundary in Fig. 1F), and resulted in unsuccessful or patchy graphene transfer.

Initially, we investigate the influence of applied force by comparing manual compression to cold lamination to cold press (up to 2 MPa) and observe its impact on the transport characteristics of PCTE supports. Next, we explore hot lamination and hot press in an effort towards mildly softening the PCTE support to promote conformal contact for enhanced graphene transfer.[53,55,56] Here, we specifically avoid temperatures >135 °C (glass transition temperature of PCTE ~147 °C) to prevent collapse of the track-etched channels in PCTE which would render it unsuitable as a porous support for membrane applications.[57] We also probe the effect of weakening the interaction of CVD graphene and the Cu substrate via water-assisted oxidation in an effort towards developing approaches for re-use of the Cu foil. Finally, we study the effect of a liquid heat spreading medium at the graphene/PCTE interface during hot lamination. The choice of isopropanol as the liquid medium is based on following criteria: *i)* the liquid must easily evaporate at temperatures <135°C and ideally leave no residue;[51,58] *ii)* the liquid must be compatible with both graphene and target PCTE substrate;[51] *iii)* the liquid should have a low surface tension to fully spread and wet the PCTE/G interface.[9,51,58–60] We note that IPA has been used to promote adhesion between graphene and TEM grids over micron scale areas[51] but to the best of our knowledge it has not been used for transfer of

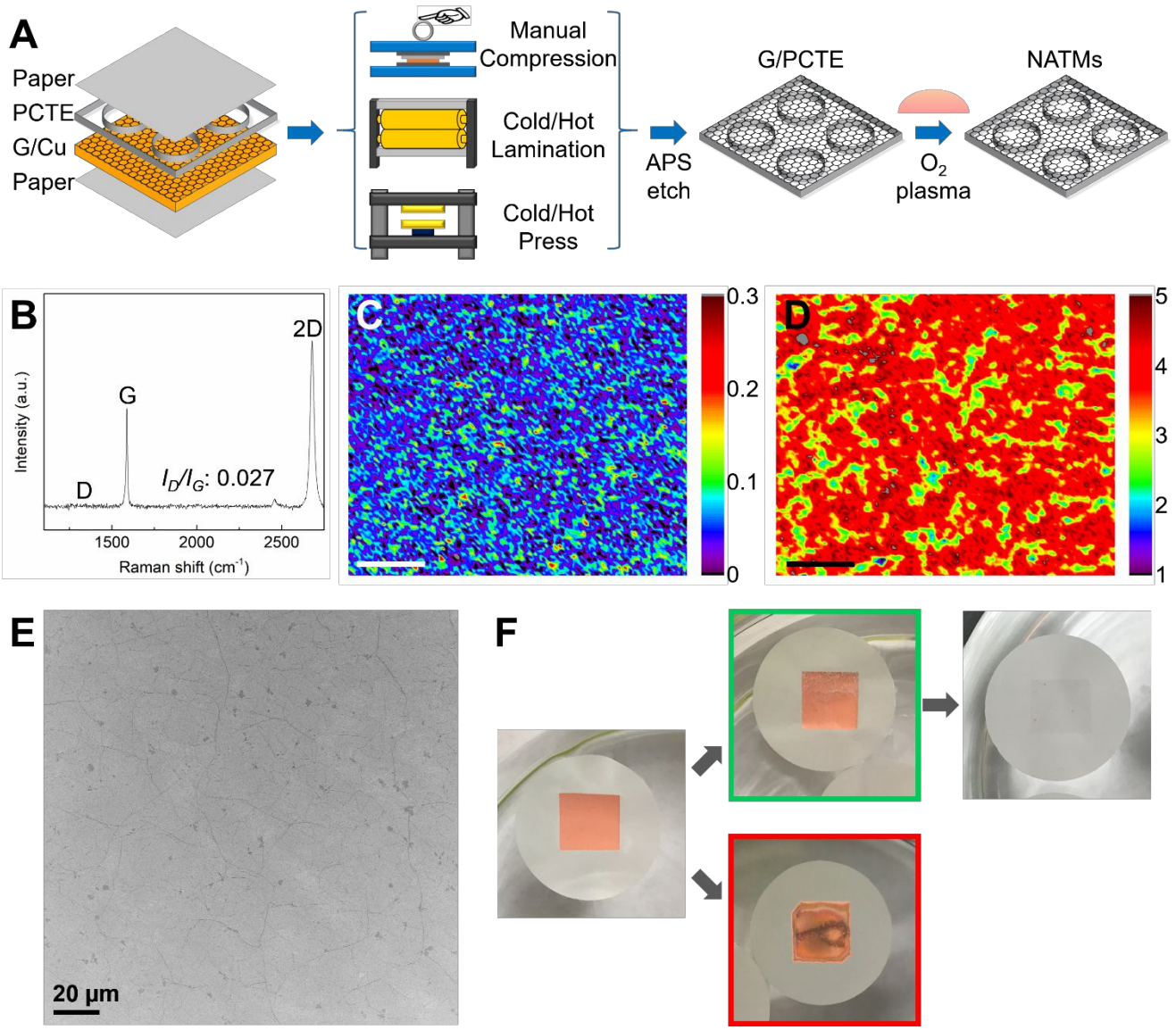

Fig. 1 Scalable synthesis of nanoporous atomically thin membranes (NATMs) for dialysis and molecular separations (A) Schematic of NATM fabrication process. PCTE support placed on graphene on Cu foil (G/Cu) is sandwiched between two pieces of weighing paper and subjected to manual compression, cold/hot lamination, and cold/hot press. Subsequent etch of the Cu allows for graphene transfer to PCTE. Finally, O_2 plasma is used to introduce nanopores and synthesize fully-functional graphene membranes. (B) Raman spectrum of high-quality graphene transferred to SiO_2 (300 nm)/Si wafer. (C) I_D/I_G and (D) I_{2D}/I_G ratios computed from Raman maps for the as-synthesized graphene. Scale bar: 50 µm. (E) SEM image of CVD graphene on copper foil. Dark lines show wrinkles indicating a continuous film. (F) Images of PCTE/G/Cu during Cu etching. Avoiding APS solution wicking in at the interface between graphene and PCTE is essential for graphene transfer.

large-area graphene to porous supports specifically for membrane applications.

2.1 Transport measurements through PCTE substrates to ensure post-processing integrity

Before evaluating the graphene transfer onto PCTE substrates, we assess the performance of PCTE substrates subjected to manual compression (MC), cold lamination (CL), cold press (CP), hot lamination (HL), isopropanol-assisted hot lamination (IHL), and hot press (HP) as shown in Fig. 1A. Here, bare PCTE substrates were contacted with annealed Cu foils without graphene (see experimental section) for obtaining controlled references. Next, we measured pressure-driven ethanol transport and diffusion-driven KCl transport across the treated PCTE supports (using the experimental setup in Fig. S1) to evaluate any changes in transport by computing the normalized flux *i.e.* dividing the measured flow rate with that of the untreated PCTE, respectively (Fig. S2). No significant change in the flux for ethanol and KCl was found before and after treatment (normalized flux ~1, Fig. S2) for approaches that only involved mechanical forces, *i.e.*, MC, CL and CP. These observations suggest that the applied pressure from manual compression as well as ~2 MPa for cold press at room temperature do not collapse or significantly change the parallel PCTE channels. Further, hot lamination and IPA-assisted hot lamination at 135 °C also resulted in the normalized flux ~1 for ethanol and KCl, indicating that the structure of the PCTE support is preserved. However, hot press at >100 °C and ~2 MPa, caused a significant decrease in normalized ethanol flux (~0.87), indicating some irreversible changes to the parallel, well-defined channels in PCTE and its un-suitability for large-

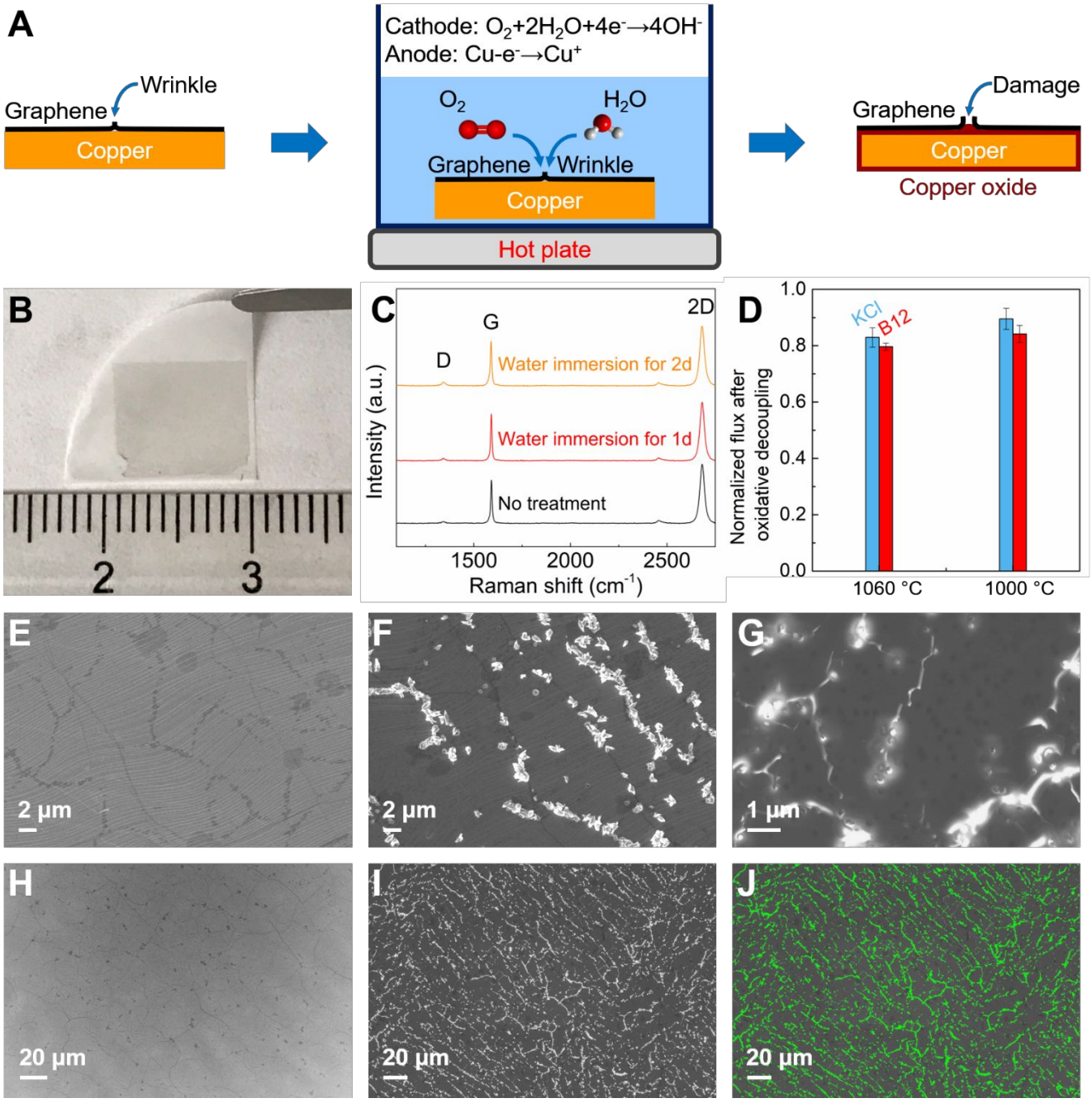

Fig. 2 Graphene transfer via water-assisted oxidation of Cu interface. (A) Schematic illustration of water-assisted oxidation process. (B) Photograph of centimeter-scale, decoupled graphene transferred to PCTE. (C) Raman spectra of graphene with no treatment and after water-assisted oxidation of Cu via immersion in water at 90 °C for 24 and 48 hours. (D) Normalized diffusive flux of 1060 °C graphene + PCTE and 1000 °C graphene + PCTE membranes fabricated after water-assisted oxidation. Error bars indicate one standard deviation. SEM image of graphene on Cu (E) before and (F) after water-assisted oxidation. (G) SEM image of graphene transferred on PCTE substrate after water-assisted oxidation of Cu. Uncovered ~200nm PCTE pores and uncovered charged polymer surfaces appear brighter. Low-magnification SEM image of graphene on Cu before (H) and after (I) water-assisted oxidation. (J) Graphene damage along wrinkles in low-magnification SEM image quantified using ImageJ threshold tool (green color).

area NATM fabrication. Hence, we exclude the hot press approach from further studies and proceed with evaluating the efficacy of approaches that do not change the structure of PCTE supports, *i.e.*, MC, CL, CP, HL, and IHL.

2.2 Water-assisted oxidation to decouple CVD graphene from Cu and facilitate transfer

Next, we explore water assisted oxidation to effectively decouple CVD graphene from Cu surface and allow for facile transfer with effective re-use of the Cu foil.[61–65] The oxidation initially starts via *i)* reaction of the Cu surfaces uncovered by graphene (*i.e.* foil edges, defects in wrinkles, and areas under defects in graphene) with ambient atmosphere as well as *ii)* oxygen intercalation between the graphene and Cu via defects.[62] Subsequently, oxidation reaction involving Cu, H_2O and oxygen (from dissolved oxygen[61,62] or water splitting[65]) takes place with graphene acting as the cathode ($O_2 + 2H_2O + 4e^- \rightarrow 4OH^-$)[61,62] and Cu working as the anode ($Cu - e^- \rightarrow Cu^+$).[62] The OH^- ions produced diffuse and meet the Cu^+ ions to

form copper oxide and/or hydroxides at the interface, thereby decoupling CVD graphene from Cu surface.[61,62]

We systematically studied decoupling of CVD graphene from Cu foil (Fig. 2A) by dipping it in a water bath at elevated temperatures to allow for water-assisted oxidation of Cu before transfer to PCTE via MC.[61,65,66] As shown in Fig. 2B, the optical image after transfer shows a uniform dark square[67,68] and clear boundary on PCTE substrate, indicating relatively good graphene transfer. However, Raman spectra of graphene measured after water assisted oxidation at 90 °C for 24 and 48 hours showed a marginal increase in I_D/I_G ratio to 0.05 and 0.08, respectively (Fig. 2C, see corresponding maps of I_D/I_G and I_{2D}/I_G ratios in Fig. S3), potentially indicating an increase in defects in the graphene.

A comparison of SEM images of graphene on Cu before and after water-assisted oxidation (Fig. 2E-J), shows bright spots and tears primarily along graphene wrinkles, indicating damages to graphene. SEM image of graphene transferred onto PCTE after water-assisted oxidation (Fig. 2G) also shows tears, open PCTE pores and uncovered PCTE (bright regions from polymer charging) along features similar to graphene wrinkles further indicating graphene damage. We estimate the overall graphene damage fractions ~10% area, from low-magnification SEM images of graphene on Cu before (Fig. 2H) and after (Fig. 2I and J) water-assisted oxidation. Specifically, the bright regions in Fig. 2I account for ~10% of area, which is larger than original graphene wrinkle fraction ~3% of area. We attribute the increase in areal damage to ruptures and damage to surrounding areas from volumetric expansion due to the growth of copper oxide/hydroxide crystals along the wrinkles.[62] Our results indicate that although decoupling of CVD graphene from Cu via water assisted oxidation aids transfer, it is typically accompanied by ~10% areal damage to graphene.[14,15,25,45,69,70]

The high fractional leakage for KCl (~0.66 nm) and Vitamin B12 (B12, ~1-1.5 nm) at ~83% and 80% respectively (Fig. 2D), compared to ~65% for KCl and ~45% for B12 using manual compression without water-assisted oxidation (Fig. 3B) further confirms damage to graphene. Finally, similar results were obtained for two independent graphene samples synthesized at different temperatures (~89% for KCl and ~84% for B12, Fig. 2D), confirming damage from the water-assisted oxidation.

2.3 Probing transport through the synthesized atomically thin graphene membranes

To quantitatively assess the performance of the centimeter-scale atomically thin graphene membranes fabricated via MC, CL, CP, HL, and IHL (see dark square in the images[67,68] in Fig. 3A), we measure pressure-driven ethanol transport and diffusion-driven transport after transfer to PCTE.

Here, we leverage the well-defined PCTE pore geometry and note that pressure-driven flow across a PCTE scales as $\sim D_P^4/L$ and diffusion-driven flow scales as D_P^2/L, where D_P is the PCTE pore diameter (~200 nm), and L is the PCTE pore length (~10 µm, thickness of PCTE).[12,45,46] For a pore in graphene with diameter D_G, pressure-driven flow scales as D_G^3, and diffusion-driven flow scales as D_G.[12,45,46] Hence, a defect D_G ~50 nm or ~4 nm will offer similar resistance as a PCTE pore D_P to pressure-driven or diffusion-driven flow, respectively.[31,43] Hence, our experiments probe three distinct size ranges of defects D_G in the fabricated centimeter-scale atomically thin graphene membranes: *i)* large tears (>50 nm) introduced from graphene transfer will offer no resistance to both pressure-driven or diffusion-driven flow respectively;[12,45,46] *ii)* small defects from a few nanometer to 50 nm will mainly block pressure-driven flow while offering almost no resistance to diffusion-driven flow;[12,45,46] *iii)* small nanopores (<4 nm) will almost completely block pressure-driven flow and also offer some resistance to diffusion-driven flow.[9,12,14,15,45,46]

Initially, we measured pressure-driven flow of ethanol through PCTE+G membranes fabricated via MC. As shown in Fig. 3B, a normalized ethanol flux of ~19% indicates a graphene coverage (defined as 100% - leakage%) of ~81%, which is in good agreement with the graphene coverage (~60-80%) previously obtained using similar MC approaches.[45] The fractional leakage of ethanol represents the percentage of large tears (>50 nm) originating from graphene transfer and handling. Diffusion-driven transport on the same membrane shows normalized flux of KCl ~65% and B12 ~45%, respectively, indicating the fractions of small tears/nanopores (1-50 nm) is ~26% and sub-nanometer scale defects (0.66-1 nm) are ~ 20%, respectively. Graphene membrane fabricated by CL also showed similar characteristics (ethanol ~19.3%, KCl ~65.6% and B12 ~45.7%) with marginal differences in the normalized fluxes (Fig. 3B) compared to membrane fabricated via MC, which indicates similar quality of transfer for both methods. The normalized fluxes for graphene membranes fabricated by CP also showed fractional leakages of KCl ~66% and B12 ~45.3%, but the fractional leakage of ethanol decreases to ~16% (Fig. 3B). These changes indicate that higher mechanical pressure ~2 MPa, slightly improves the graphene transfer quality on PCTE.

Graphene membranes fabricated using HL, showed normalized flux of ethanol ~15%, KCl ~61%, and B12 ~41%, respectively (Fig. 3B). The ~4% drop (compared to PCTE+G transferred by MC or CL) in fractional leakage suggests improved transfer with HL, probably due to the mild softening of PCTE with temperature ~135℃ resulting in enhanced contact between graphene and PCTE.[53]

Interestingly, for graphene membranes fabricated via IHL, the fractional leakages for all species decreased drastically (ethanol ~0.802%, KCl ~26%, and B12 ~14%), indicating significantly improved (>99%) graphene transfer. Further, we also measured the diffusion-driven transport of Lysozyme (Lz, ~3.8-4 nm) and obtained a fractional leakage of ~4%, demonstrating that the majority of leakage (~22%) can be attributed to defects <4 nm (fractional leakage of KCl – fractional leakage of Lz). These small defects can only allow for fractional ethanol leakage of ~0.002% (calculated from pressure-driven flow scaling), and hence the remaining ~0.8% of leakage originates from ≥50 nm defects in graphene and/or tears introduced during transfer. SEM images of the fabricated graphene membranes (Fig. 3D-G) further confirm these observations, *i.e. i)* for areas with no wrinkles, the graphene film appears to be uniformly transferred onto PCTE substrate and no defects/tears are visible (Fig. 3F); *ii)* for areas with wrinkles, some wrinkles overlap the PCTE pores but do not contain defects/tears (Fig. 3D, E and G) and *iii)* in some cases wrinkles overlapping on PCTE pores show defects >50 nm or tears primarily along the wrinkles (Fig. 3D and G). We note that wrinkles account for ~3% of the graphene area, and hence assign the ~0.8%

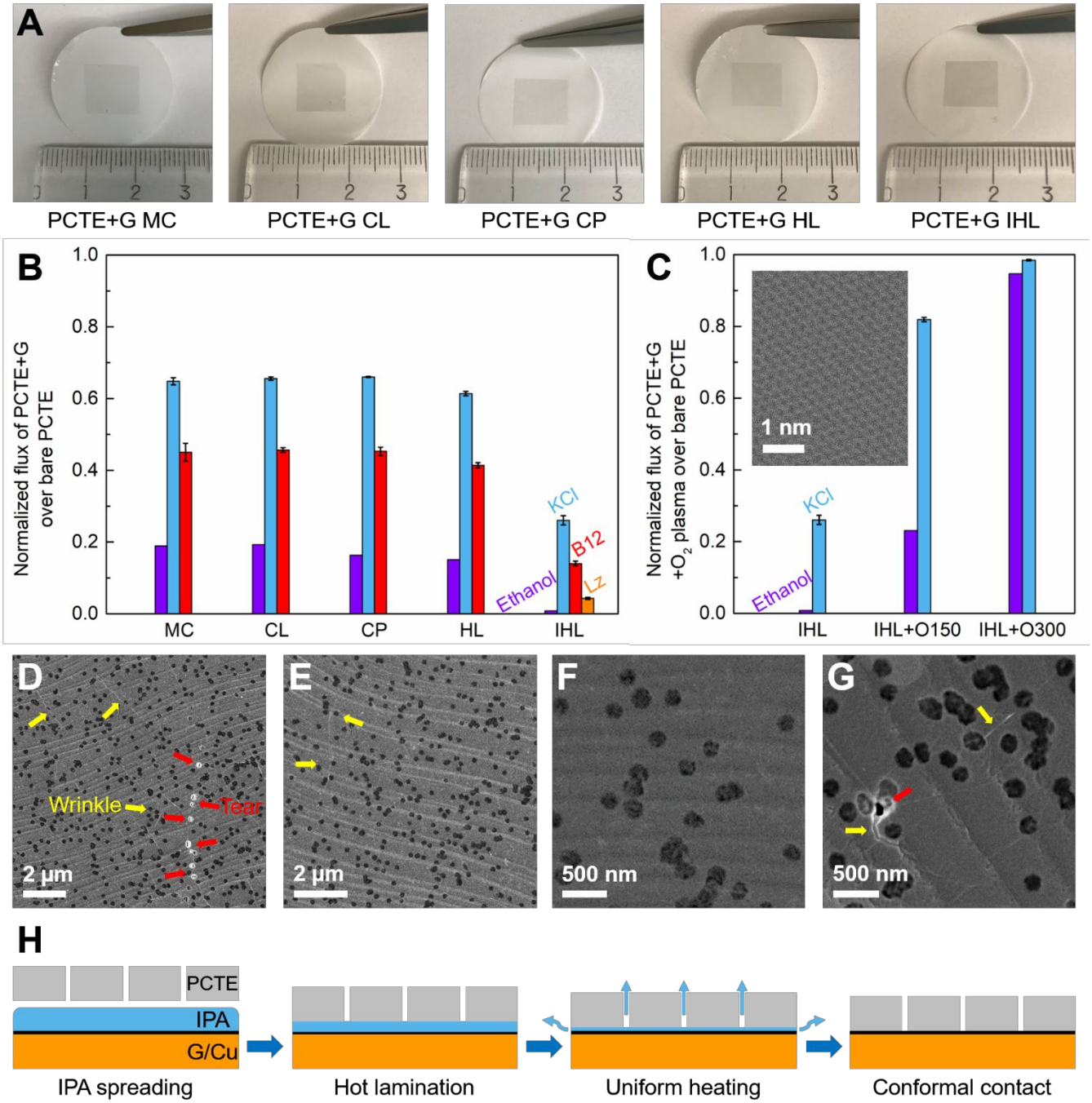

Fig. 3 Assessment of the synthesized atomically thin membranes. (A) Photographs of graphene transferred to PCTE substrates via manual compression (MC), cold lamination (CL), cold press (CP), hot lamination (HL), and isopropanol-assisted hot lamination (IHL) approaches. (B) Normalized flux of pressure-driven flow with ethanol and diffusion-driven flow with KCl (~0.66 nm), B12 (~1-1.5nm) and Lz (~3.8-4nm) for graphene transferred to PCTE using different approaches. Note G +PCTE membrane transferred by IHL exhibits the lowest transport and hence the highest transfer yield. (C) Normalized flux of pressure-driven flow with ethanol and diffusion-driven flow with KCl as a function of O_2 plasma time for PCTE+G membrane transferred by IHL. Error bars indicate one standard deviation. Inset: STEM image of as-synthesized graphene transferred to TEM grids using IPA shows significant regions of the graphene surface remain atomically clean. (D-G) SEM images of graphene transferred onto PCTE substrates. Yellow arrows represent graphene winkles, while red arrows show tears and small pores primarily along wrinkles. (H) Schematic of the proposed mechanism for IHL graphene transfer.

of ethanol leakage to defects >50 nm or tears in graphene primarily along wrinkles (since not all wrinkles overlap the PCTE pores). Taken together, our observations indicate that in comparison to MC or CL, IHL significantly increases the graphene transfer yield from 81% to 99.2% and to the best of our knowledge represents the highest values reported for centimeter-scale atomically thin membranes to this date.

To further confirm the efficacy of the IHL method and unambiguously assign the measured transport to graphene, we systematically etched the graphene on PCTE with O_2 plasma and measured transport through it. As shown in Fig. 3C, the normalized flux of ethanol and KCl respectively increase to ~23% and ~82% after O_2 plasma etch for 150 s, confirming that the transport behavior observed in Fig. 3B can be clearly attribute to graphene. O_2 plasma

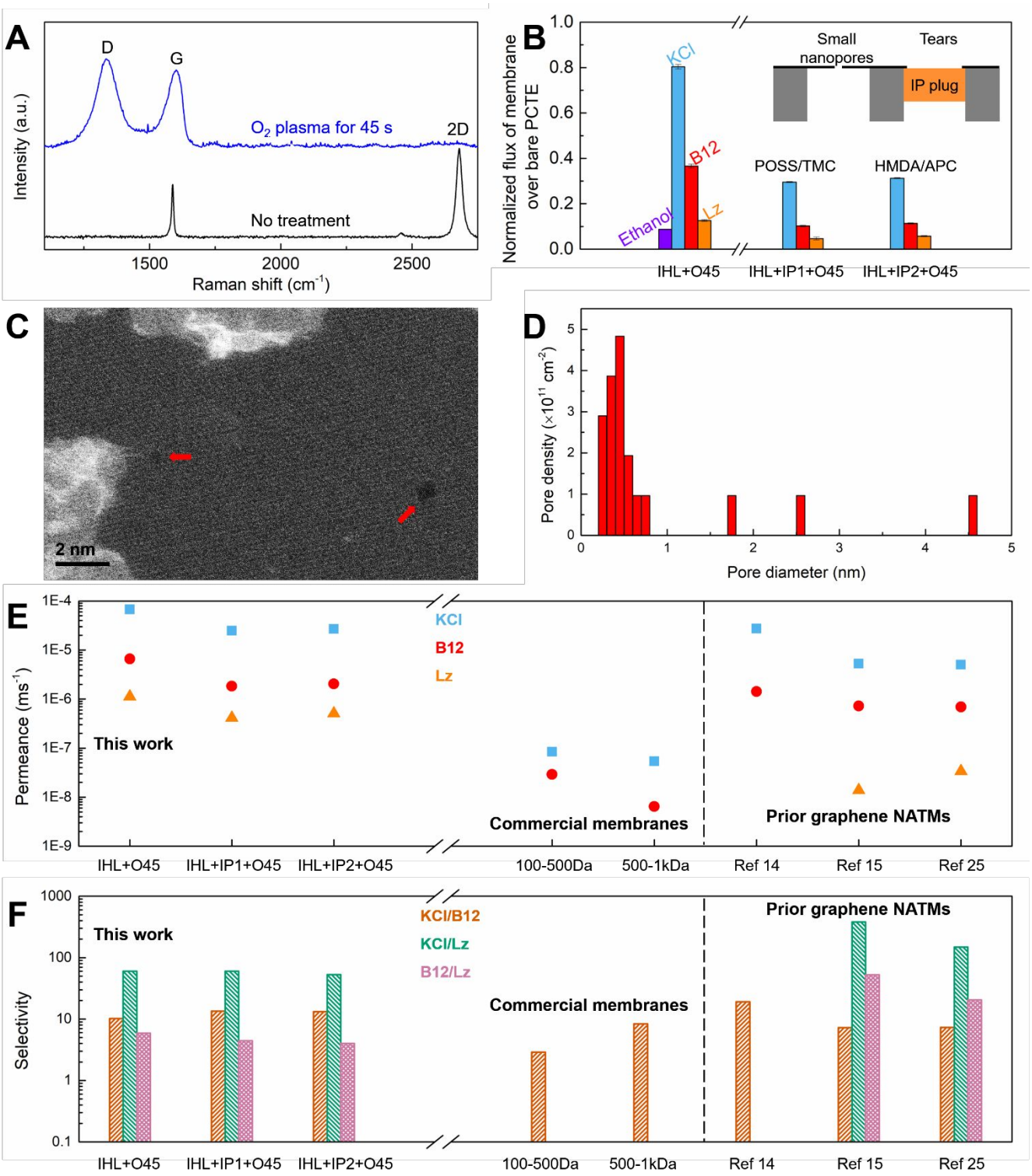

Fig. 4 Assessment of fully functional centimeter-scale graphene NATMs. (A) Raman spectra of graphene without and with O_2 plasma etch for 45s. (B) Normalized flux of pressure-driven flow with ethanol and diffusion-driven flow with KCl, B12 and Lz for PCTE+graphene+O_2 plasma 45 s, PCTE+graphene+ IP1 (POSS/TMC) +O_2 plasma 45 s and PCTE+graphene+ IP2 (HMDA/APC) +O_2 plasma 45 s membranes. All membranes are transferred by IHL. Error bars indicate one standard deviation. Inset shows schematic of the interfacial polymerization (IP) process. (C) STEM image acquired on graphene after O_2 plasma etch for 45s (red arrows indicate representative nanopores). (D) Pore size distribution of graphene with O_2 plasma etch for 45s. (E) Diffusive permeance of the fabricated NATMs compared with commercially available dialysis membranes (100-500Da and 500-1000Da) and prior work on NATMs (taken from Ref. 14, Ref. 15, and Ref. 25) for KCl, B12 and Lz. Note permeance is calculated by taking into account the 10% porosity of PCTE supports (also see Fig. S4). (F) Selectivity (ratio of permeance of two species) for the membranes in E.

etch for ~300s further damages graphene, and results in ~95% of ethanol leakage and ~99% of KCl leakage (Fig. 3C). These control experiments clearly demonstrate that the observed transport can be attributed to monolayer graphene and that the PCTE channels

remain un-affected after IHL, since the results are fully consistent with the control experiments performed on bare PCTE (see Fig. S2).

Additionally, we also transferred graphene to TEM grids with holey carbon with IPA (see experimental section) followed by thermal annealing, and confirmed that significant regions of the graphene surface remained atomically clean after IPA evaporation (see inset of STEM image in Fig. 3C), despite the presence of amorphous carbon from holey carbon in the grids as well as exposure to adventitious carbon from atmospheric exposure after annealing.

We attribute the significant improvement in graphene transfer via IHL to IPA that acts as a liquid heat transfer medium and propose the following mechanism (Fig. 3H). IPA introduced at the PCTE/G interface spreads evenly over the entire contact area, forming a thin liquid layer between graphene and PCTE substrate.[9,51,58–60] Upon hot lamination at ~135 °C, the IPA functions as an effective thermal transmission layer to provide uniform heat transfer throughout the PCTE/G interface. As hot lamination proceeds, IPA on the edges and directly under PCTE support pores/channels start to evaporate, but will be quickly replenished by IPA from the interior and nearby areas,[71,72] thereby maintaining a relatively even IPA film thickness between graphene and PCTE substrate. Consequently, the gap between graphene and PCTE substrate slowly decreases all over the contact area, and PCTE substrate makes uniform contact with graphene on Cu foil almost simultaneously.[72] Finally, the IPA completely evaporates (leaving a very clean surface),[51,58] surface tension, together with applied mechanical force and heat treatment, draw graphene and PCTE substrate into intimate contact allowing for facile fabrication of centimeter-scale atomically thin membranes that is fully compatible with roll-to-roll manufacturing.[51,59]

2.4 Centimeter-scale NATMs for dialysis and molecular separations

Finally, we demonstrate fully functional centimeter-scale NATMs for dialysis and molecular separations using facile O_2 plasma etch (see experimental section) of PCTE+G membrane fabricated by IHL. As shown in Fig. 4A, after 45 s of O_2 plasma etch, a large D peak appears in the Raman spectrum of graphene while 2D peak almost completely disappears, indicating the formation of defects that manifest as sub-nanometer to nanometer pores in the graphene lattice (see Fig. 4C).[14,54] These nanopores allow for selective molecular transport through IHL+O45 membrane (Fig. 4B, PCTE+G+O_2 plasma 45 s). Compared to the PCTE+G transferred IHL (Fig. 3B), the normalized flux of KCl of the IHL+O45 membrane (Fig. 4B) significantly increases to 80.4%, while the normalized flux of B12 and Lz mildly increase to 36.6% and 12.6%, respectively. These changes indicate that the majority of pores created via 45 s of O_2 plasma etch are sub-nanometer pores. Atomic resolution scanning transmission electron microscopy (STEM, Fig. 4C) provides direct evidence for the existence of nanopores in the graphene lattice after 45 s of O_2 plasma etching. The corresponding pore size distribution (Fig. 4D) also confirms that the majority of nanopores are <1 nm, with few large nanopores ~1-5 nm with an overall nanopore density is $\sim 1.84 \times 10^{12}$ cm^{-2}.

A comparison of solute permeance (see experimental section) and selectivity (ratio of solute permeance) of IHL+O45 membrane with state-of-the-art commercial dialysis membranes (molecular weight cut-offs specified at 100-500 Da and 500-1000 Da),[14] indicates our NATMs not only exhibit ~2-3 orders of magnitude higher permeance, but also offer better or at least comparable selectivity for KCl/B12 separation, indicating their potential for de-salting of small molecule and small proteins via dialysis (see Fig. 4E and Fig. S4).

Most importantly, the functional performance of centimeter-scale IHL+O45 membrane, was realized without any interfacial polymerization (IP) based sealing approaches (see inset in Fig. 4B) typically used prior to nanopore creation, indicating the advantages of high transfer yields ≥99.2% and the choice of PCTE supports with minimal pore overlap in facile and scalable NATM fabrication.[9,14] Control NATMs using two different IP based sealing processes *i.e.* IHL+IP1+O45 and IHL+IP2+O45 (see methods) show normalized flux of KCl, B12 and Lz ~29.5%, ~10.2%, ~4.7% and ~31.2%, ~11.3%, ~5.7%, respectively (Fig. 4B). Compared to these membranes with IP (IHL+IP1+O45 and IHL+IP2+O45), the synthesized IHL+O45 membrane show higher permeance (Fig. 4E) while offering similar selectivity for the desalting and molecular separations (Fig. 4F). We also note that the IHL+O45 membrane outperforms graphene NATMs from prior studies (Fig. 4E). These results indicate our facile and scalable IHL approach allows for the fabrication of fully functional large-area graphene NATMs for practical applications in desalting and molecular separations for drug purifications, biochemical analytics, and dialysis, especially in the 100-1000 Da range.

3 Conclusions

In summary, we systematically investigated the factors influencing facile and scalable NATM fabrication via transfer of CVD graphene from a Cu foil onto PCTE supports via MC, MP and scalable lamination approaches. We show that MC, CL, CP, HL and IHL enable facile and clean transfer of large-area graphene onto a PCTE support without compromising support porosity/integrity. Particularly, our novel roll-to-roll manufacturing compatible IHL process allows for the graphene transfer yield ≥99.2% and is one of the highest values reported to this date for centimeter-scale atomically thin membranes. The remaining 0.8% leakage is attributed to ≥ 50 nm defects and/or tears primarily along wrinkles in CVD graphene. Furthermore, water-assisted oxidation effectively decouples CVD graphene from the Cu foil, and aids graphene transfer, but also results in ~10% areal graphene damage along wrinkles. Finally, we demonstrate fully functional centimeter-scale graphene NATMs that show ~2-3 orders of magnitude higher permeance than state-of-the-art commercially available dialysis membranes with better or at least comparable selectivity, and outperforms prior graphene NATMs. Our work provides a novel, facile and scalable roll-to-roll manufacturing compatible approach for the fabrication of fully-functional large-area NATMs that present potential for transformative advances in dialysis, molecular separations, ionic/molecular transport, and beyond.

4 Experimental section

4.1 Graphene growth

Unless specified otherwise graphene was synthesized on Cu foils at 1050 °C using low-pressure chemical vapor deposition (LPCVD) as reported in detail elsewhere.[14,15,25,45] The Cu foil (99.9% purity, 18 µm thick, JX Holding HA) was pre-treated with diluted nitric acid (20%) via sonication for 4 min to remove surface oxides and contaminants, followed by washing with deionized (DI) water and drying in air. For graphene synthesis at 1050-1060 °C, the Cu foil was annealed in a hot-walled tube furnace (1 inch) at 1050 °C for 60 min under 500 sccm H_2 (~60 Torr), and then grown under 3.5 sccm CH_4 and 250 sccm H_2 for 30 min, followed by another 30 min of growth with 7 sccm CH_4 and 250 sccm H_2. Finally, the Cu foil was quench-cooled to room temperature in the same growth atmosphere.[14,15,25,45] For obtaining annealed Cu foil without graphene, the same recipe was used without introducing any CH_4 precursor.

4.2 Graphene transfer to PCTE substrates

Before transfer, CVD graphene on Cu foil was pre-etched in 0.1 M of ammonium persulfate (APS) solution for 30 min to remove graphene on the bottom side of Cu foil, followed by rinsing in DI water (two times, 10 min per time) and drying in air.[14,15,25,45] Polycarbonate track etch (PCTE, Sterlitech, ~10% porosity, 10 µm thick, hydrophobic, polyvinylpyrrolidone-free, Lot # 7072229) substrate were also washed in pure ethanol (Sigma Aldrich, 200 proof) and dried in air. Subsequently, PCTE was placed against the graphene/Cu foil (G/Cu) with graphene side facing up, and sandwiched between two pieces of weighing paper to make a paper/PCTE/G/Cu/paper stack.

For graphene transfer using manual compression approach,[14,15,25,45] the stack was sandwiched between two glass slides and compressed with light finger pressure using a glass Pasteur pipette tube as the roller at room temperature. For graphene transfer using cold/hot lamination, the stack was sandwiched between two protective Teflon films and then laminated at room temperature or 135 °C using a TruLam TL-320B roll-to-roll compatible laminator. A thin layer of isopropanol (IPA) solvent (50 µL) was added to the PCTE/G interface as the liquid heat transfer medium when using IPA-assisted hot lamination approach. For graphene transfer using cold/hot press, the Teflon/paper/PCTE/G/Cu/paper/Teflon stack was compressed under 2 MPa at room temperature or 100 °C for 4 min using a Driptech Press. Subsequently, the PCTE/G/Cu was gently made to float on APS solution to completely etch Cu. Finally, the PCTE/G stack was rinsed with DI water to remove the APS residue, followed by rinsing in ethanol and drying in air.[14,15,25,45]

Similar methods were employed to press bare PCTE substrates against annealed Cu foil without graphene for obtaining treated PCTE references.

For graphene transfer with water-assisted oxidation, CVD graphene on Cu foil was immersed in DI water at 90 °C for 24 - 48 hours, and then transferred to PCTE using the manual compression approach described above.

4.3 Graphene transfer to SiO_2/Si wafer for Raman spectroscopy

Graphene transfer to SiO_2/Si wafers was performed using polymethyl methacrylate (PMMA) assisted transfer method.[14,15,25,45] Before the transfer, CVD graphene was pre-etched in APS solution (0.2 M) for 10 min to remove graphene on the bottom side of Cu foil, followed by rinsing in DI water for 10 min and drying in air. PMMA (2% in anisole) was drop-casted on to graphene side of the Cu foil and allowed to dry at room temperature. Next, the Cu foil was completely etched in APS solution (0.2 M), and the PMMA/graphene stack was rinsed with DI water for 10 min. Finally, the stack was transferred to a SiO_2 (300 nm)/Si wafer, followed by washing in acetone and cleaning in IPA.

4.4 Graphene transfer to TEM grids

Graphene transfer to TEM grids (Ted Pella Inc. 658-200-AU with 1.2 µm holes) was carried out using the method reported elsewhere with some modifications.[9,13,51,58,73] The TEM grid was placed onto the graphene on Cu foil (pre-etched as described above) with the Quantifoil carbon film facing down and[14,15,25,45] IPA (10 µL) was used to wet the interface. After drying for 2 h, the stack was annealed at 80 °C on a hotplate for 30 min to enhance adhesion. Finally, the Cu foil was completely etched in APS solution, rinsed in two subsequent DI water baths, followed by rinsing with IPA and drying in air.[9,13,51,58,73]

4.5 Oxygen plasma treatment

Oxygen plasma etching was performed in a plasma cleaner (Harrick Plasma PDC-001, maximum RF power of 30 W) under 500 mTorr at low RF power setting to etch graphene.

4.6 Interfacial polymerization

Interfacial polymerization was carried out based on the methods detailed elsewhere.[14,15,19,25,45,69,70] Before the reaction, PCTE + graphene stack was annealed at 105 °C for 12 hours. IP1 process was performed with a Franz cell (PermeGear, Inc.) using octa ammonium polyhedral oligomeric silsesquioxane (POSS, Hybrid Plastics, AM0285) in water (aqueous phase) and trimesoyl chloride (TMC, Alfa Aesar, 4422-95-1) in hexane (organic phase),[25] while IP2 process used hexamethylene diamine (HMDA, Sigma-Aldrich 165212) in water (aqueous phase) and adipoyl chloride (APC, Alfa Aesar, 124-09-4) in hexane (organic phase).[9,14]

4.7 Characterization

SEM images of graphene on Cu foils and on PCTE substrates were acquired with a Zeiss Merlin Scanning Electron Microscope with Gemini II Column operated at 2-5 kV.

Raman spectra were recorded using a Thermo Scientific DXR Confocal Raman spectrometer with a 532 nm laser source at a laser power of 1 mW. Raman mapping was performed using a Renishaw InVia Raman microscope at the Center for Nanophase Materials Sciences at Oak Ridge National Laboratory and the Wire software was used for data analysis.

STEM imaging was performed with Nion UltraSTEM 100 aberration-corrected scanning transmission electron microscope (STEM), operated at 60 kV at the Center for Nanophase Materials Sciences at Oak Ridge National Laboratory.[14,15,25,45] The samples on TEM grids were vacuum-annealed at 160 °C for 12 hours before imaging.[14,15,25,45]

4.8 Transport measurements

Pressure-driven ethanol transport and diffusion-driven solute transport measurements were all carried out as reported in detail elsewhere.[9,12–15,25,45,46] The setup used for transport measurements was a customized 7 mL Side-Bi-Side glass diffusion cell (PermeGear, Inc.) with a 5 mm orifice (Fig. S1). The feed solution was always introduced on the left cell (graphene side) and magnetic Teflon coated stir bars vigorously stirred both cells.[9,12–15,25,45,46]

For pressure-driven transport measurement,[45,46] the system was washed with pure ethanol before measurement. Both cells were then filled with ethanol, and a height difference in ethanol was used to induce a hydrostatic head. The drop in the ethanol meniscus level along the graduated syringe from 250 µL was recorded with a digital camera every 60s. Ethanol permeance was calculated by $permeance = (\Delta V/\Delta P)/(\Delta t \times A_{effective})$, where ΔV is the ethanol volume change, ΔP is the pressure difference across the membrane, Δt is the time interval, and $A_{effective}$ is the effective membrane area in the transport process. The ratio of the ethanol permeance for each fabricated membrane with respect to bare PCTE substrate was computed to obtain the normalized flux.[12,45,46]

For diffusion-driven transport measurement, the system was washed with DI water for five times (5 min per time) to completely remove ethanol residue after ethanol transport measurement. [9,12–15,25,45,46] Three model solutes were specifically selected for the transport measurement: KCl (Fisher Chemical, 7447-40-7, 74.55 Da), Vitamin B12 (B12, Sigma-Aldrich, 68-19-9, 1355 Da), and Lysozyme (Lz, VWR, 12650-88-3, 14300 Da). For measuring KCl transport, 0.5 M of KCl solution was filled into the left cell (feed side), and DI water was filled into the right cell (permeate side) in which a probe of conductivity meter (Mettler Toledo SevenCompact S230) was immersed for recording the conductivity values every 15s for 15 min.[9,12–15,25,45,46]

For measuring the transport of organic molecules (B12 and Lz), 1mM of organic molecule solution in 0.5 M KCl was filled into the left cell (feed side), and 0.5 M KCl solution was filled into the right cell (permeate side) in which a fiber optic probe attached to a UV-vis Spectrophotometer (Agilent Cary 60) collected absorbance spectra in the range of 190 to 1100 nm every 15s for 40 min.[9,12–15,25,45,46] The UV-vis peak positions we used for measuring the intensity differences are as follows: 710 nm for DI water (reference wavelength), 360 nm for B12, and 282 nm for Lz. The transport rate of each solute was measured by calculating the slope of concentration change in the permeate side (right side). The ratio of the rate of concentration change (slops) for each fabricated membrane with respect to bare PCTE substrate was computed to obtain the normalized flux.[9,12–15,25,45,46] All measurements were replicated three times.

Solute (KCl, B12 and Lz) permeance was calculated by $permeance = (V \times dC/dt)/(\Delta C \times A_{effective})$, where V is the volume of diffusion cell (7 mL), dC/dt is the slope of concentration change in the permeate side, ΔC is concentration difference between feed side and permeate side, and $A_{effective}$ is the effective area of membranes (accounting for 10% porosity of PCTE). Solute/solute selectivity between different species was obtained by calculating the ratio of solute permeance.

Conflicts of interest

P.R.K. declares stake in a company aimed at commercializing application from 2D materials.

Author contributions

P.C. and P.R.K. conceived the idea. P.R.K. supervised the project. P.C. performed transfer and transport experiments and analyzed the results. N.K.M. prepared high quality CVD graphene and contributed to graphene characterizations. J.-C.I. performed scanning transmission electron microscopy imaging. I.N.I. performed Raman mapping. P.C. and P.R.K. wrote the manuscript with input from all co-authors.

Acknowledgments

The use of Vanderbilt Institute of Nanoscale Science and Engineering CORE facilities is acknowledged. This work was supported by ACS PRF Grant number 59267-DNI10, NSF CAREER award #1944134, and faculty start-up funds to P.R.K. from Vanderbilt University. The STEM imaging and Raman mapping were performed at the Center for Nanophase Materials Sciences at Oak Ridge National Laboratory, a U.S. Department of Energy Office of Science User Facility. We acknowledge Andrew E. Naclerio for assistance with the hot press experiments and Mattigan M. Kelly and Dahsong Lee for assistance with imaging for the ethanol transport experiments.

Notes and references

1 J. C. Meyer, A. K. Geim, M. I. Katsnelson, K. S. Novoselov, T. J. Booth and S. Roth, *Nature*, 2007, **446**, 60–63.

2 L. Wang, M. S. H. Boutilier, P. R. Kidambi, D. Jang, N. G. Hadjiconstantinou and R. Karnik, *Nat. Nanotechnol.*, 2017, **12**, 509–522.

3 L. Prozorovska and P. R. Kidambi, *Adv. Mater.*, 2018, **30**, 1801179.

4 S. Huang, M. Dakhchoune, W. Luo, E. Oveisi, G. He, M. Rezaei, J. Zhao, D. T. L. Alexander, A. Züttel, M. S. Strano and K. V. Agrawal, *Nat. Commun.*, 2018, **9**, 2632.

5 M. S. H. Boutilier, D. Jang, J.-C. Idrobo, P. R. Kidambi, N. G. Hadjiconstantinou and R. Karnik, *ACS Nano*, 2017, **11**, 5726–5736.

6 D. Jiang, V. R. Cooper and S. Dai, *Nano Lett.*, 2009, **9**, 4019–4024.

7 S. Choi, S. H. Tan, Z. Li, Y. Kim, C. Choi, P. Y. Chen, H. Yeon, S. Yu and J. Kim, *Nat. Mater.*, 2018, **17**, 335–340.

8 Y. Yang, X. Yang, L. Liang, Y. Gao, H. Cheng, X. Li, M. Zou, R. Ma, Q. Yuan and X. Duan, *Science*, 2019, **364**, 1057–1062.

9 S. C. O'Hern, D. Jang, S. Bose, J.-C. Idrobo, Y. Song, T. Laoui, J. Kong and R. Karnik, *Nano Lett.*, 2015, **15**, 3254–3260.

10 D. Jang, J.-C. Idrobo, T. Laoui and R. Karnik, *ACS Nano*, 2017, **11**, 10042–10052.

11 S. P. Surwade, S. N. Smirnov, I. V Vlassiouk, R. R. Unocic, G.

M. Veith, S. Dai and S. M. Mahurin, *Nat. Nanotechnol.*, 2015, **10**, 459–464.
12 S. C. O'Hern, C. A. Stewart, M. S. H. Boutilier, J.-C. Idrobo, S. Bhaviripudi, S. K. Das, J. Kong, T. Laoui, M. Atieh and R. Karnik, *ACS Nano*, 2012, **6**, 10130–10138.
13 S. C. O'Hern, M. S. H. Boutilier, J.-C. Idrobo, Y. Song, J. Kong, T. Laoui, M. Atieh and R. Karnik, *Nano Lett.*, 2014, **14**, 1234–1241.
14 P. R. Kidambi, D. Jang, J.-C. Idrobo, M. S. H. Boutilier, L. Wang, J. Kong and R. Karnik, *Adv. Mater.*, 2017, **29**, 1700277.
15 P. R. Kidambi, G. D. Nguyen, S. Zhang, Q. Chen, J. Kong, J. Warner, A.-P. Li and R. Karnik, *Adv. Mater.*, 2018, **30**, 1804977.
16 T. Jain, B. C. Rasera, R. J. S. Guerrero, M. S. H. Boutilier, S. C. O'Hern, J.-C. Idrobo and R. Karnik, *Nat. Nanotechnol.*, 2015, **10**, 1053–1057.
17 R. C. Rollings, A. T. Kuan and J. A. Golovchenko, *Nat. Commun.*, 2016, **7**, 11408.
18 R. M. Wyss, T. Tian, K. Yazda, H. G. Park and C.-J. Shih, *Nano Lett.*, 2019, **19**, 6400–6409.
19 P. Cheng, M. M. Kelly, N. K. Moehring, W. Ko, A.-P. Li, J. C. Idrobo, M. S. H. Boutilier and P. R. Kidambi, *Nano Lett.*, , DOI:10.1021/acs.nanolett.0c01934.
20 L. Cantley, J. L. Swett, D. Lloyd, D. A. Cullen, K. Zhou, P. V Bedworth, S. Heise, A. J. Rondinone, Z. Xu, S. Sinton and J. S. Bunch, *Nanoscale*, 2019, **11**, 9856–9861.
21 S. Hu, M. Lozada-Hidalgo, F. C. Wang, A. Mishchenko, F. Schedin, R. R. Nair, E. W. Hill, D. W. Boukhvalov, M. I. Katsnelson, R. A. W. Dryfe, I. V Grigorieva, H. A. Wu and A. K. Geim, *Nature*, 2014, **516**, 227–230.
22 S. Bukola, Y. Liang, C. Korzeniewski, J. Harris and S. Creager, *J. Am. Chem. Soc.*, 2018, **140**, 1743–1752.
23 G. F. Schneider, S. W. Kowalczyk, V. E. Calado, G. Pandraud, H. W. Zandbergen, L. M. K. Vandersypen and C. Dekker, *Nano Lett.*, 2010, **10**, 3163–3167.
24 C. A. Merchant, K. Healy, M. Wanunu, V. Ray, N. Peterman, J. Bartel, M. D. Fischbein, K. Venta, Z. Luo, A. T. C. Johnson and M. Drndić, *Nano Lett.*, 2010, **10**, 2915–21.
25 P. R. Kidambi, D. D. Mariappan, N. T. Dee, A. Vyatskikh, S. Zhang, R. Karnik and A. J. Hart, *ACS Appl. Mater. Interfaces*, 2018, **10**, 10369–10378.
26 S. Bae, H. Kim, Y. Lee, X. Xu, J.-S. Park, Y. Zheng, J. Balakrishnan, T. Lei, H. Ri Kim, Y. Il Song, Y.-J. Kim, K. S. Kim, B. Özyilmaz, J.-H. Ahn, B. H. Hong and S. Iijima, *Nat. Nanotechnol.*, 2010, **5**, 574–578.
27 X. Li, W. Cai, J. An, S. Kim, J. Nah, D. Yang, R. Piner, A. Velamakanni, I. Jung, E. Tutuc, S. K. Banerjee, L. Colombo and R. S. Ruoff, *Science*, 2009, **324**, 1312 LP – 1314.
28 M. Chen, R. C. Haddon, R. Yan and E. Bekyarova, *Mater. Horizons*, 2017, **4**, 1054–1063.
29 Y.-C. Lin, C. Jin, J.-C. Lee, S.-F. Jen, K. Suenaga and P.-W. Chiu, *ACS Nano*, 2011, **5**, 2362–2368.
30 J.-Y. Hong, Y. C. Shin, A. Zubair, Y. Mao, T. Palacios, M. S. Dresselhaus, S. H. Kim and J. Kong, *Adv. Mater.*, 2016, **28**, 2382–2392.
31 H. H. Kim, B. Kang, J. W. Suk, N. Li, K. S. Kim, R. S. Ruoff, W. H. Lee and K. Cho, *ACS Nano*, 2015, **9**, 4726–4733.
32 W. S. Leong, H. Wang, J. Yeo, F. J. Martin-Martinez, A. Zubair, P.-C. Shen, Y. Mao, T. Palacios, M. J. Buehler, J.-Y. Hong and J. Kong, *Nat. Commun.*, 2019, **10**, 867.
33 M. M. Tavakoli, G. Azzellino, M. Hempel, A.-Y. Lu, F. J. Martin-Martinez, J. Zhao, J. Yeo, T. Palacios, M. J. Buehler and J. Kong, *Adv. Funct. Mater.*, 2020, **n/a**, 2001924.
34 A. Pirkle, J. Chan, A. Venugopal, D. Hinojos, C. W. Magnuson, S. McDonnell, L. Colombo, E. M. Vogel, R. S. Ruoff and R. M. Wallace, *Appl. Phys. Lett.*, 2011, **99**, 122108.
35 M. Kratzer, B. C. Bayer, P. R. Kidambi, A. Matković, R. Gajić, A. Cabrero-Vilatela, R. S. Weatherup, S. Hofmann and C. Teichert, *Appl. Phys. Lett.*, 2015, **106**, 103101.
36 J. Meyer, P. R. Kidambi, B. C. Bayer, C. Weijtens, A. Kuhn, A. Centeno, A. Pesquera, A. Zurutuza, J. Robertson and S. Hofmann, *Sci. Rep.*, 2015, **4**, 5380.
37 S. Sanders, A. Cabrero-Vilatela, P. R. Kidambi, J. A. Alexander-Webber, C. Weijtens, P. Braeuninger-Weimer, A. I. Aria, M. M. Qasim, T. D. Wilkinson, J. Robertson, S. Hofmann and J. Meyer, *Nanoscale*, 2015, **7**, 13135–42.
38 A. Kuruvila, P. R. Kidambi, J. Kling, J. B. Wagner, J. Robertson, S. Hofmann and J. Meyer, *J. Mater. Chem. C*, 2014, **2**, 6940.
39 P. R. Kidambi, C. Weijtens, J. Robertson, S. Hofmann and J. Meyer, *Appl. Phys. Lett.*, 2015, **106**, 063304.
40 A. Winter, Y. Ekinci, A. Gölzhaüser and A. Turchanin, *2D Mater.*, 2019, **6**, 021002.
41 Y.-C. Lin, C.-C. Lu, C.-H. Yeh, C. Jin, K. Suenaga and P.-W. Chiu, *Nano Lett.*, 2012, **12**, 414–419.
42 C. Gong, H. C. Floresca, D. Hinojos, S. McDonnell, X. Qin, Y. Hao, S. Jandhyala, G. Mordi, J. Kim, L. Colombo, R. S. Ruoff, M. J. Kim, K. Cho, R. M. Wallace and Y. J. Chabal, *J. Phys. Chem. C*, 2013, **117**, 23000–23008.
43 P. R. Kidambi, C. Ducati, B. Dlubak, D. Gardiner, R. S. Weatherup, M.-B. Martin, P. Seneor, H. Coles and S. Hofmann, *J. Phys. Chem. C*, 2012, **116**, 22492–22501.
44 P. R. Kidambi, B. C. Bayer, R. Blume, Z.-J. Wang, C. Baehtz, R. S. Weatherup, M.-G. Willinger, R. Schloegl and S. Hofmann, *Nano Lett.*, 2013, **13**, 4769–4778.
45 P. R. Kidambi, R. A. Terry, L. Wang, M. S. H. Boutilier, D. Jang, J. Kong and R. Karnik, *Nanoscale*, 2017, **9**, 8496–8507.
46 P. R. Kidambi, M. S. H. Boutilier, L. Wang, D. Jang, J. Kim and R. Karnik, *Adv. Mater.*, 2017, **29**, 1605896.
47 K. Celebi, J. Buchheim, R. M. Wyss, A. Droudian, P. Gasser, I. Shorubalko, J.-I. Kye, C. Lee and H. G. Park, *Science*, 2014, **344**, 289–292.
48 Z. Yuan, J. D. Benck, Y. Eatmon, D. Blankschtein and M. S. Strano, *Nano Lett.*, 2018, **18**, 5057–5069.
49 M. Caglar, I. Silkina, B. T. Brown, A. L. Thorneywork, O. J. Burton, V. Babenko, S. M. Gilbert, A. Zettl, S. Hofmann and U. F. Keyser, *ACS Nano*, 2020, **14**, 2729–2738.
50 K. Choi, A. Droudian, R. M. Wyss, K.-P. Schlichting and H. G. Park, *Sci. Adv.*, 2018, **4**, eaau0476.
51 W. Regan, N. Alem, B. Alemán, B. Geng, Ç. Girit, L. Maserati, F. Wang, M. Crommie and A. Zettl, *Appl. Phys. Lett.*, 2010, **96**, 113102.

52 Y. Qin, Y. Hu, S. Koehler, L. Cai, J. Wen, X. Tan, W. L. Xu, Q. Sheng, X. Hou, J. Xue, M. Yu and D. Weitz, *ACS Appl. Mater. Interfaces*, 2017, **9**, 9239–9244.

53 L. G. P. Martins, Y. Song, T. Zeng, M. S. Dresselhaus, J. Kong and P. T. Araujo, *Proc. Natl. Acad. Sci.*, 2013, **110**, 17762 LP – 17767.

54 A. C. Ferrari and D. M. Basko, *Nat. Nanotechnol.*, 2013, **8**, 235–246.

55 G. J. M. Fechine, I. Martin-Fernandez, G. Yiapanis, R. Bentini, E. S. Kulkarni, R. V Bof de Oliveira, X. Hu, I. Yarovsky, A. H. Castro Neto and B. Özyilmaz, *Carbon N. Y.*, 2015, **83**, 224–231.

56 W. Jung, D. Kim, M. Lee, S. Kim, J.-H. Kim and C.-S. Han, *Adv. Mater.*, 2014, **26**, 6394–6400.

57 Datasheet of PCTE Membrane, Sterlitech, https://www.sterlitech.com/hydrophobic-polycarbonate-membrane-filter-pctf0225100.html, (accessed 5 May 2020).

58 J. Park, H. Elmlund, P. Ercius, J. M. Yuk, D. T. Limmer, Q. Chen, K. Kim, S. H. Han, D. A. Weitz, A. Zettl and A. P. Alivisatos, *Science*, 2015, **349**, 290.

59 W.-H. Lin, T.-H. Chen, J.-K. Chang, J.-I. Taur, Y.-Y. Lo, W.-L. Lee, C.-S. Chang, W.-B. Su and C.-I. Wu, *ACS Nano*, 2014, **8**, 1784–1791.

60 J. Chan, A. Venugopal, A. Pirkle, S. McDonnell, D. Hinojos, C. W. Magnuson, R. S. Ruoff, L. Colombo, R. M. Wallace and E. M. Vogel, *ACS Nano*, 2012, **6**, 3224–3229.

61 R. Wang, P. R. Whelan, P. Braeuninger-Weimer, S. Tappertzhofen, J. A. Alexander-Webber, Z. A. Van Veldhoven, P. R. Kidambi, B. S. Jessen, T. Booth, P. Bøggild and S. Hofmann, *ACS Appl. Mater. Interfaces*, 2016, **8**, 33072–33082.

62 R. Wu, L. Gan, X. Ou, Q. Zhang and Z. Luo, *Carbon*, 2016, **98**, 138–143.

63 A. Shivayogimath, P. R. Whelan, D. M. A. Mackenzie, B. Luo, D. Huang, D. Luo, M. Wang, L. Gammelgaard, H. Shi, R. S. Ruoff, P. Bøggild and T. J. Booth, *Chem. Mater.*, 2019, **31**, 2328–2336.

64 K. Wong, S. J. Kang, C. W. Bielawski, R. S. Ruoff and S. K. Kwak, *J. Am. Chem. Soc.*, 2016, **138**, 10986–10994.

65 D. Luo, X. You, B.-W. Li, X. Chen, H. J. Park, M. Jung, T. Y. Ko, K. Wong, M. Yousaf, X. Chen, M. Huang, S. H. Lee, Z. Lee, H.-J. Shin, S. Ryu, S. K. Kwak, N. Park, R. R. Bacsa, W. Bacsa and R. S. Ruoff, *Chem. Mater.*, 2017, **29**, 4546–4556.

66 J. Kim, H. Park, J. B. Hannon, S. W. Bedell, K. Fogel, D. K. Sadana and C. Dimitrakopoulos, *Science*, 2013, **342**, 833 LP – 836.

67 K. F. Mak, M. Y. Sfeir, Y. Wu, C. H. Lui, J. A. Misewich and T. F. Heinz, *Phys. Rev. Lett.*, 2008, **101**, 196405.

68 R. R. Nair, P. Blake, A. N. Grigorenko, K. S. Novoselov, T. J. Booth, T. Stauber, N. M. R. Peres and A. K. Geim, *Science*, 2008, **320**, 1308 LP – 1308.

69 Y. Zhang, N. E. Benes and R. G. H. Lammertink, *Lab Chip*, 2015, **15**, 575–580.

70 M. Dalwani, J. Zheng, M. Hempenius, M. J. T. Raaijmakers, C. M. Doherty, A. J. Hill, M. Wessling and N. E. Benes, *J. Mater. Chem.*, 2012, **22**, 14835–14838.

71 R. D. Deegan, O. Bakajin, T. F. Dupont, G. Huber, S. R. Nagel and T. A. Witten, *Nature*, 1997, **389**, 827–829.

72 H. H. Kim, S. K. Lee, S. G. Lee, E. Lee and K. Cho, *Adv. Funct. Mater.*, 2016, **26**, 2070–2077.

73 M. R. Au - Hauwiller, J. C. Au - Ondry and A. P. Au - Alivisatos, *JoVE*, 2018, e57665.